

Elasticity, shear strength, and equation of state of molybdenum and gold from x-ray diffraction under nonhydrostatic compression to 24 GPa

Thomas S. Duffy

Department of Geosciences, Princeton University, Princeton, New Jersey 08544

Guoyin Shen

Consortium for Advanced Radiation Sources, The University of Chicago, 5640 South Ellis Avenue, Chicago, Illinois 60637

Jinfu Shu, Ho-Kwang Mao, and Russell J. Hemley

Geophysical Laboratory and Center for High-Pressure Research, Carnegie Institution of Washington, 5251 Broad Branch Road NW, Washington, DC 20015

Anil K. Singh

Materials Science Division, National Aerospace Laboratories, Bangalore 5600 17, India

(Received 7 June 1999; accepted for publication 10 September 1999)

Lattice strains were measured as a function of the angle ψ between the diffracting plane normal and the stress axis of a diamond anvil cell in a layered sample of molybdenum and gold. The sample was compressed over the range 5–24 GPa and the lattice strains were measured using energy-dispersive x-ray diffraction. As ψ is varied from 0° to 90° , the mean lattice parameter of molybdenum increases by up to 1.2% and that of gold increases by up to 0.7%. A linear relationship between $Q(hkl)$, which is related to the slope of the measured d spacing versus $1 - 3 \cos^2 \psi$ relation, and $3\Gamma(hkl)$, a function of the Miller indices of the diffracting plane, is observed for both materials as predicted by theory. The pressure dependence of the uniaxial stress t for gold from this and other recent studies is given by $t = 0.06 + 0.015P$, where P is the pressure in GPa. The uniaxial stress in molybdenum can be described by $t = 0.46 + 0.13P$. Using gold as an internal pressure standard, the equation of state of molybdenum depends strongly on ψ . The bulk modulus obtained from a Birch–Murnaghan fit varies from 210 to 348 GPa as ψ varies from 0° to 90° . However, an equation of state in good agreement with shock and ultrasonic isotherms is obtained for $\psi = 54.7^\circ$ where the deviatoric contribution to the lattice strain vanishes. Second-order elastic moduli for gold and molybdenum are obtained from the data. The results are generally consistent with an earlier x-ray study and with extrapolations of low-pressure ultrasonic data. The pressure dependence of the shear modulus C_{44} is smaller for the x-ray data than predicted by extrapolation of ultrasonic data. © 1999 American Institute of Physics. [S0021-8979(99)03524-0]

I. INTRODUCTION

Molybdenum is a body-centered-cubic (bcc) transition metal whose high-pressure behavior has attracted considerable experimental and theoretical interest.^{1–6} Shock compression experiments have been carried out over a wide pressure range and qualify molybdenum for use as a secondary pressure standard.^{7,8} Static compression has been carried out to 272 GPa and the bcc structure is stable to at least this pressure,³ although under shock loading there is evidence for a phase transition at 210 GPa.^{2,4} First-principles theoretical equation of state calculations have also been carried out over a wide P – T interval.⁵ The pressure dependences of the single-crystal elastic moduli of molybdenum have been measured ultrasonically to 0.5 GPa in a nitrogen pressure medium⁹ and theoretical calculations of the elastic moduli to very large compressions ($V/V_0 = 0.4$) have been reported using the local-density approximation.⁶

Molybdenum is one of four metals (Cu, Mo, Pd, Ag) whose reduced shock isotherms were used to calibrate the ruby fluorescence pressure scale,¹ which is a widely used secondary pressure scale for diamond-anvil cell experiments.

The effect of shear strength on both the dynamic and static compression curves is one important source of error in the ruby scale. Originally, no correction for strength effects was made because the static and dynamic strengths were poorly constrained. Subsequently, it has been shown that shocked metals retain significant shear strength up to 100 GPa (Refs. 10 and 11) due to viscous dislocation drag and spontaneous nucleation of point defects. The yield strength of molybdenum was measured under dynamic loading both at room temperature¹² and from a 1400 °C initial temperature.¹³ Because of large differences in temperature and strain rate, the strength of static and dynamically compressed materials may differ. There is thus a strong need to characterize the static strength of metals used as standards in shock and static compression studies.

Gold is a face-centered-cubic (fcc) noble metal that is widely used as a secondary pressure calibrant in static experiments¹⁴ and was used to calibrate the quasihydrostatic ruby pressure scale to 180 GPa.¹⁵ However, reported values of the pressure dependence of the individual elastic moduli from ultrasonic elasticity measurements at elevated

pressures^{16–19} are inconsistent and this discrepancy has not been resolved. The uncertainty in pressure determination when using gold as a secondary standard is $\sim 5\%–10\%$ as a result of this uncertainty.²⁰

Here, we examine molybdenum and gold under nonhydrostatic compression to 24 GPa. Using theories^{21–23} describing lattice strains in an opposed anvil device together with experimental techniques^{24–26} that allow measurement of strain at any orientation relative to the stress axis, it is possible to constrain material properties such as shear strength, the elasticity tensor, and the quasihydrostatic compression curve from x-ray diffraction measurements under nonhydrostatic loading. The technique also yields information on properties of the sample environment such as the stress tensor, texturing, and stress/strain continuity across grain boundaries.

II. THEORY

The theory describing lattice strains in a sample nonhydrostatically compressed in the diamond-anvil cell has been discussed elsewhere.^{21–24,26,27} Here, we restrict ourselves to a summary of the main features.

The sample in a diamond-anvil cell is held in a small gasket hole and compressed uniaxially between two gem-quality diamonds. The stress tensor in the center of a diamond cell sample can be written as

$$\begin{aligned} \sigma &= \begin{bmatrix} \sigma_1 & 0 & 0 \\ 0 & \sigma_1 & 0 \\ 0 & 0 & \sigma_3 \end{bmatrix} \\ &= \begin{bmatrix} \sigma_p & 0 & 0 \\ 0 & \sigma_p & 0 \\ 0 & 0 & \sigma_p \end{bmatrix} \\ &+ \begin{bmatrix} -t/3 & 0 & 0 \\ 0 & -t/3 & 0 \\ 0 & 0 & 2t/3 \end{bmatrix}, \end{aligned} \quad (1)$$

where σ_3 is the principal stress in the axial or diamond cell load direction, σ_1 is the principal stress in the radial direction, and σ_p is the mean normal stress or pressure. The difference between the maximum (σ_3) and minimum (σ_1) stresses is the uniaxial stress component t , which is taken to be positive on compression,

$$t = \sigma_3 - \sigma_1 = 2\tau = Y, \quad (2)$$

where τ is the shear strength and Y the yield strength of the material. The latter two equalities in Eq. (2) hold for a Von Mises yield condition and depend on conditions of plastic flow being reached. In fact, t could be less than the yield strength.

The d spacing for a given set of lattice planes measured by x-ray diffraction is a function of the angle ψ between the diamond cell stress axis and the diffracting plane normal (Fig. 1):

$$d_m(hkl) = d_p(hkl)[1 + (1 - 3 \cos^2 \psi)Q(hkl)], \quad (3)$$

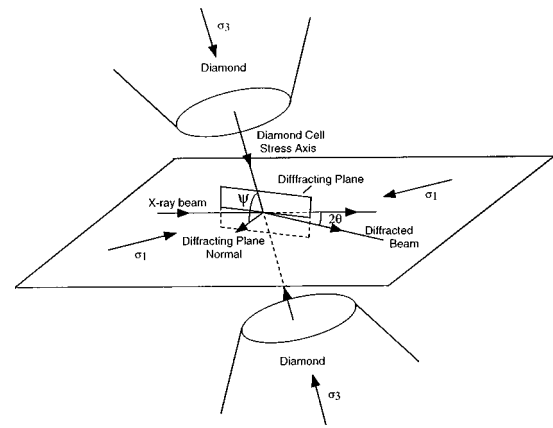


FIG. 1. Experimental geometry for radial diffraction experiments. ψ is the angle between the diamond cell stress axis and the diffracting plane normal.

where $d_m(hkl)$ and $d_0(hkl)$ are the measured d spacings for the lattice plane (hkl) under compression and at ambient pressure, respectively, $d_p(hkl)$ is the interplanar spacing that would result under application of hydrostatic pressure σ_p alone, and $Q(hkl)$ is given by

$$Q(hkl) = \frac{t}{3} \left[\frac{\alpha}{2G_R(hkl)} + \frac{1 - \alpha}{2G_V} \right]. \quad (4)$$

$G_R(hkl)$ is the aggregate shear modulus for the crystallites contributing to the diffracted intensity entering the detector under the condition of constant stress across grain boundaries (Reuss limit). G_V is the Voigt (constant strain) bound on the aggregate shear modulus and is not orientation dependent. The parameter α , which varies between 0 and 1, specifies the degree of stress and strain continuity across grains in the sample.

For the cubic system,

$$(2G_R)^{-1} = S_{11} - S_{12} - 3S_{44}\Gamma(hkl), \quad (5)$$

where S , a measure of the elastic anisotropy, is given by

$$S = S_{11} - S_{12} - S_{44}/2, \quad (6)$$

and

$$\Gamma(hkl) = \frac{h^2k^2 + k^2l^2 + h^2l^2}{(h^2 + k^2 + l^2)^2}, \quad (7)$$

and

$$(2G_V)^{-1} = \frac{5}{2} \frac{(S_{11} - S_{12})S_{44}}{[3(S_{11} - S_{12}) + S_{44}]}, \quad (8)$$

where the S_{ij} are the single-crystal elastic compliances.

According to Eq. (3), $d_m(hkl)$ should vary linearly with $1 - 3 \cos^2 \psi$. The intercept of the relation ($\psi = 54.7^\circ$) gives the d spacing due to the hydrostatic component of the stress. At this angle, there is no contribution to the measured d spacing from the deviatoric stress tensor. The slope of the $d_m(hkl)$ vs $1 - 3 \cos^2 \psi$ relation yields the product $d_p(hkl)Q(hkl)$.

Equations (4)–(6) also predict a linear relationship between $Q(hkl)$ and $3\Gamma(hkl)$ with slope m_1 and intercept m_0 given by

$$m_0 = \frac{t}{3}[S_{11} - S_{12}], \quad (9)$$

$$m_1 = -\frac{t}{3}[S_{11} - S_{12} - S_{44}/2], \quad (10)$$

for the case where $\alpha = 1$. More general expressions that hold for any value of α are given elsewhere.²³

In addition, the linear compressibility χ of a cubic crystal is given by

$$\chi = -\left(\frac{\partial \ln a}{\partial P}\right)_T = \frac{1}{3K} = S_{11} + 2S_{12}, \quad (11)$$

where a is the lattice parameter and K is the isothermal bulk modulus.

These three expressions, together with the inverse relationship between the elastic stiffness and elastic compliance tensors,²⁸ can be used to write the following expressions for the isothermal elastic stiffnesses C_{ij} of a cubic crystal:

$$C_{11} = \frac{1}{3\chi} + \frac{2t}{9m_0}, \quad (12)$$

$$C_{12} = \frac{1}{3\chi} - \frac{t}{9m_0}, \quad (13)$$

$$C_{44} = \frac{t}{6(m_0 + m_1)}. \quad (14)$$

Thus, by measuring the dependence of interplanar spacing on the angle from the diamond cell stress axis under nonhydrostatic compression, the single-crystal stiffness tensor can be constrained. In addition, it is also possible to recover the d spacing and, hence, lattice parameter, for the hydrostatic component of the stress tensor. To solve Eqs. (12)–(14), it is necessary to know the uniaxial stress t as well as the axial compressibility.

Using Eq. (4), the uniaxial stress component can be determined from

$$t = 6G\langle Q(hkl) \rangle, \quad (15)$$

where $\langle Q(hkl) \rangle$ represents the average value over all observed reflections. The pressure dependence of G can be obtained from extrapolation of ultrasonic or other single-crystal elasticity data. Equation (15) is strictly true only for elastically isotropic materials but t has been shown to depend only weakly on combinations of α and anisotropy.²³

III. EXPERIMENTAL TECHNIQUE

Experiments were conducted using energy-dispersive synchrotron x-ray diffraction at the bending magnet beamline (13-BM-A) of the GSECARS sector at the Advanced Photon Source. The sample consisted of high-purity molybdenum powder with a thin gold layer on the upper surface. The sample was contained within a 40 μm hole in a beryllium gasket and compressed using a diamond-anvil cell.

Incident x rays were collimated by a pair of tungsten carbide slits and focused to 10 $\mu\text{m} \times 10 \mu\text{m}$ with Kirkpatrick–Baez optics. The size of the incident x-ray beam was measured using a sharp edge. Both the incident and

diffracted beams passed through the 6-mm-diam beryllium gasket which absorbs little of the high-energy x rays.²⁹ The sample was positioned such that the x-ray beam passed near the interface of the molybdenum and gold layers or entirely within the molybdenum layer. The diamond cell was mounted in a rotation stage on a two-circle horizontal diffractometer.³⁰ The angle ψ between the diffraction plane normal and the diamond cell stress axis was varied from 0° (diffraction plane normal parallel to the diamond cell stress axis) to 90° (diffraction plane normal perpendicular to stress axis) (Fig. 1). The diffracted beam passed through a double-slit system and was detected by a Ge solid-state detector.

At each pressure, energy-dispersive diffraction patterns were recorded at angular intervals of 5°–15° for about 5–10 min each. Diffraction patterns were recorded upon compression at seven pressures between 4.6 and 24.0 GPa and upon decompression at 19.5 and 14.7 GPa. The equivalent hydrostatic pressures were determined from the measured lattice parameter at $\psi = 54.7^\circ$ and the equation of state of gold¹⁷ as discussed below.

Peak positions were obtained by fitting background-subtracted Voigt line shapes to the spectra. For gold, the (111), (200), (220), (311), (222), (400), and (331) diffraction lines were used. For Mo, the analysis was based on the following diffraction lines: (110), (200), (211), (220), and (310).

The method used here differs from conventional energy-dispersive diffraction experiments in which the incident and diffracted x-ray beams pass through the diamond-anvils. Due to the limited x-ray access afforded by the diamond seats, ψ can be varied only over a small range near $\sim 85^\circ$ in the conventional geometry. Thus, diffraction measurements are confined to near the minimum stress direction. However, by using a beryllium gasket, the diffraction vector can be positioned at any orientation relative to the diamond cell axis.

IV. RESULTS

Selected diffraction patterns for the Au–Mo sample as a function of ψ are shown in Fig. 2. The diffraction peaks shift to higher energy as the angle is decreased, reflecting the increased strain as the diffraction plane normal approaches the maximum stress axis. The peak shift is larger for the molybdenum lines than for the gold lines because of the larger uniaxial stress component sustained in the molybdenum sample. While the peak intensities are variable, there are no consistent trends in intensity as the angle is varied, suggesting that no uniform texturing is developed in these samples, unlike hcp metals.²⁶

The observed relative intensity changes may arise from local preferred orientation. Since the gold layer is very thin, changes in sample position as the cell is rotated can result in large intensity changes. Changes in peak position will only occur upon sample position changes if there are pressure gradients across the sample. The size of the sample hole was minimized to reduce this effect. The possibility of time-dependent changes in the diffraction pattern (i.e., stress relaxation) was examined by recording patterns at a particular angle at both the beginning and end of the data collection

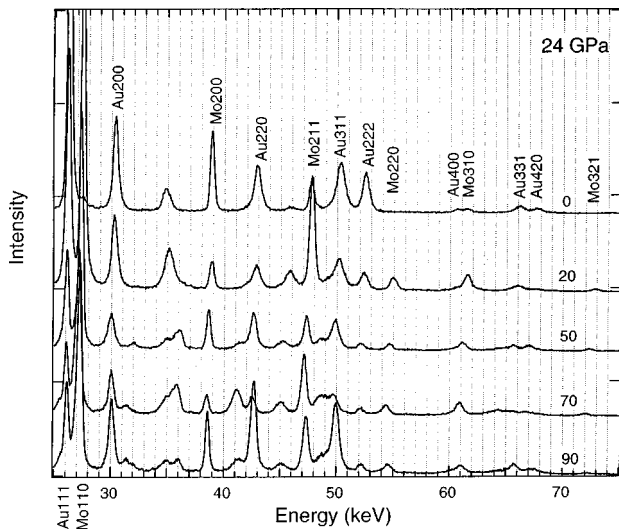


FIG. 2. Selected x-ray diffraction patterns as a function of angle from the stress axis at 24 GPa. Diffraction lines from molybdenum and gold are labeled. Unlabeled lines are from the beryllium gasket. The angle ψ , corresponding to each pattern, is shown at the right.

process for a particular pressure. No systematic changes in the diffraction pattern with time were observed.

The variation of d spacing with ψ is shown for representative diffraction lines in Fig. 3. For both molybdenum and gold, a linear relationship with $1 - 3 \cos^2 \psi$ is observed in all cases. The d spacing and lattice parameter corresponding to the purely hydrostatic component of stress, $1 - 3 \cos^2 \psi$

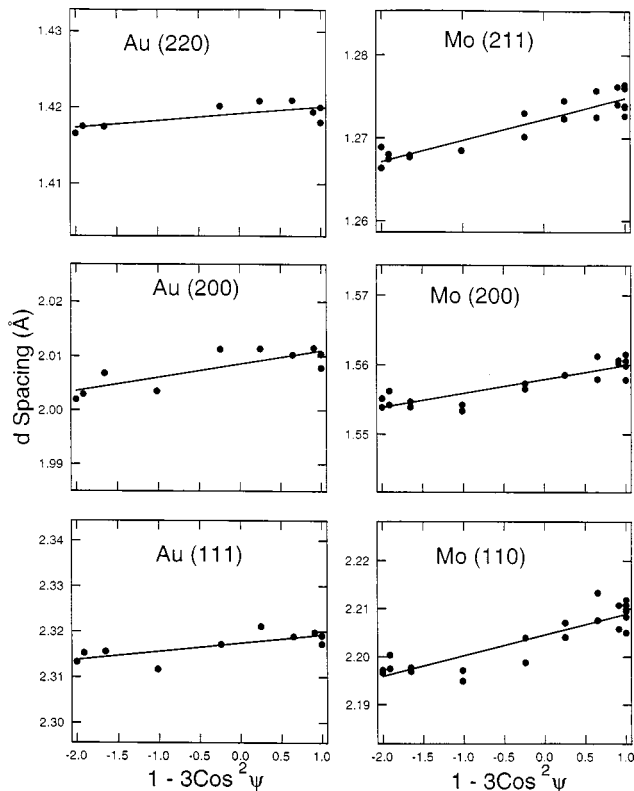


FIG. 3. Dependence of d spacing on $1 - 3 \cos^2 \psi$ for selected diffraction lines of gold and molybdenum at 9 GPa. The solid lines are least-squares fits to the data. The y-axis range is $\pm 1\%$ for each panel.

TABLE I. Lattice parameter and equation of state for gold.

$a(\psi=54.7^\circ)$ Å	V/V_0	$P(\psi=54.7^\circ)$ (GPa)	$P(\psi=90^\circ)$ (GPa)	$P(\psi=0^\circ)$ (GPa)
4.043(2)	0.9748	4.6	4.1	5.6
4.014(3)	0.9532	9.1	8.4	10.4
3.996(2)	0.9405	12.0	11.2	13.6
3.991(2)	0.9362	13.1	11.9	15.2
3.973(3)	0.9243	16.2	15.4	17.3
3.948(2)	0.9070	21.0	19.5	23.8
3.934(2)	0.8974	24.0	22.3	27.2
3.956(3) ^a	0.9125	19.4	17.9	23.1
3.985(3) ^a	0.9327	14.0	13.3	15.7

^aIndicates data taken on decompression.

$=0$ ($\psi=54.7^\circ$), was determined for each diffraction peak and mean values are shown in Tables I and II. The standard deviation of the mean lattice parameter determined from all the gold and molybdenum lines was less than 0.1% at this angle. At 0° and 90° , the standard deviation of the mean lattice parameter was larger, but still less than 0.2%.

Figure 4 shows the variation of the lattice parameter determined from the linear fits to d spacing data (Fig. 3) for each diffraction line as a function of $1 - 3 \cos^2 \psi$. For gold, the (200) line generally yields the smallest lattice parameter at $\psi=0^\circ$ and the largest lattice parameter at $\psi=90^\circ$. Conversely, the (111) line is the smallest at $\psi=90^\circ$ and the largest lattice parameter at $\psi=0^\circ$. These results are consistent with other studies.^{26,31} For molybdenum, the (110) line yields a lattice parameter that is systematically high by about 0.1% at $\psi=54.7^\circ$. The other diffraction lines tend to converge at $1 - 3 \cos^2 \psi=0$. In going from 0° to 90° , there is a 0.4%–1.1% increase in the mean molybdenum lattice parameter and a 0.2%–0.7% increase in the mean gold lattice parameter at each pressure over the 5–24 GPa pressure range.

In addition to the reduced variance of the mean lattice parameter, a reduction in the diffraction peak width tends to be observed as ψ approaches the critical value of 54.7° (Fig. 5). On average, the peaks widths are reduced by $\sim 20\%$ at $\psi=50^\circ$ – 60° , relative to $\psi=0^\circ$ and 90° . The peak width is sensitive to both the macroscopic and microscopic deviatoric stress fields.^{31,32} The reduction in width is further evidence that the total contribution of the deviatoric stress is reduced at $1 - 3 \cos^2 \psi=0$.

TABLE II. Diffraction data for molybdenum.

P (GPa)	$a(\psi=54.7^\circ)$ Å	V/V_0 ($\psi=54.7^\circ$)	$a(\psi=90^\circ)$ Å	$a(\psi=0^\circ)$ Å
4.6	3.129(1)	0.983	3.133(1)	3.121(3)
9.1	3.116(2)	0.971	3.121(3)	3.105(2)
12.0	3.105(2)	0.960	3.113(3)	3.088(3)
13.1	3.102(4)	0.958	3.111(6)	3.084(4)
16.2	3.094(2)	0.950	3.103(4)	3.074(3)
21.0	3.079(2)	0.936	3.089(3)	3.058(4)
24.0	3.071(3)	0.929	3.083(4)	3.046(3)
19.4 ^a	3.084(3)	0.941	3.096(4)	3.061(6)
14.0 ^a	3.104(4)	0.955	3.115(6)	3.083(5)

^aIndicates data taken on decompression.

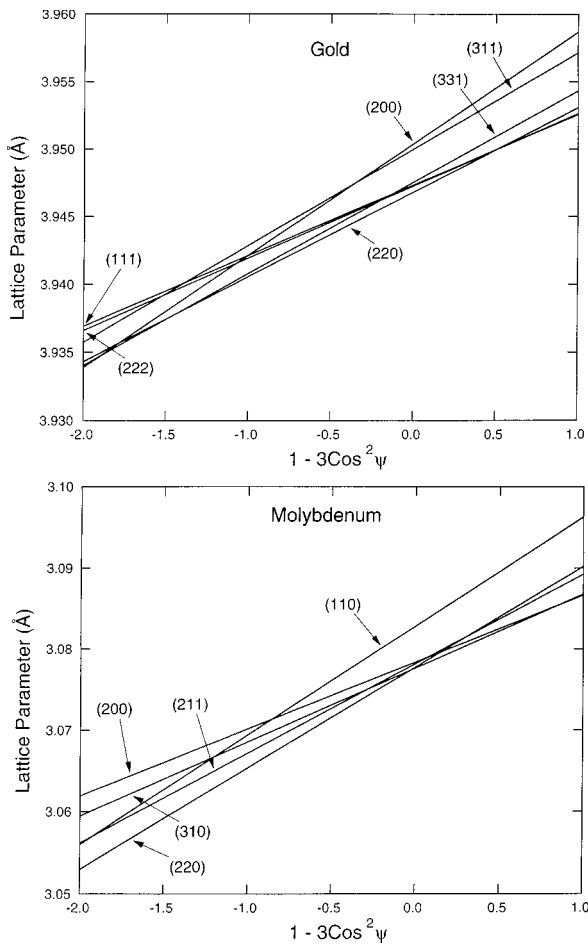


FIG. 4. Variation of lattice parameter determined from each diffraction line with angle for (a) gold and (b) molybdenum at 21.0 GPa. The solid lines are from the least-squares fits to d spacing versus $1 - 3 \cos^2 \psi$ (Fig. 3). The relative y-axis range in (b) is twice the relative y-axis range is (a).

The dependence of $Q(hkl)$ on $3\Gamma(hkl)$ is shown in Fig. 6. For both gold and molybdenum, a linear relationship is observed. The case of a bcc material is somewhat unfavorable as many of the diffraction lines yield the same value of 3Γ and the observed diffraction planes do not span the pos-

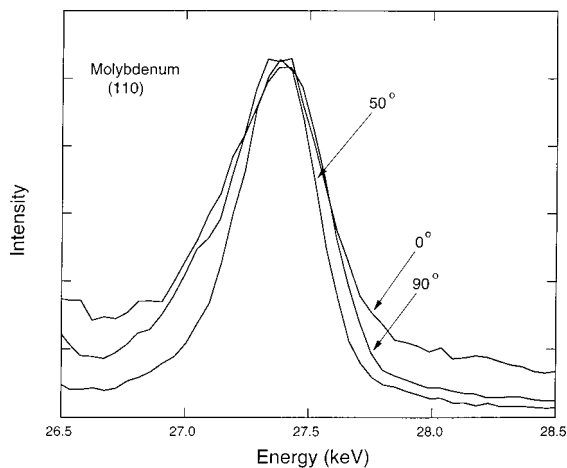


FIG. 5. Molybdenum (200) diffraction peak at selected angles. The patterns have been arbitrarily shifted in energy to align the peaks.

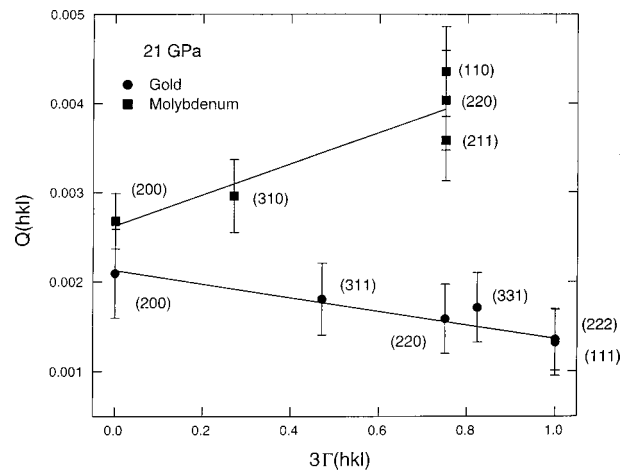


FIG. 6. $Q(hkl)$ as a function of 3Γ for gold and molybdenum at 21.0 GPa. The solid lines are least-squares fits to the data. The estimated errors on $Q(hkl)$ are obtained from the scatter of the $d(hkl)$ vs $1 - 3 \cos^2 \psi$ relation.

sible range of 3Γ values. No systematic trends are observed in the $Q(hkl)$ values for diffraction peaks which have the same value of 3Γ .

Using the equation of state of gold,¹⁷ the pressure was determined from the mean lattice parameter at 54.7° using the third-order Birch–Murnaghan equation³³ (Table I). Pressures were also calculated from the measured strains at 0° and 90° by assuming that the lattice strain in this direction represents the hydrostatic strain (Table I). The pressures inferred from strain measurements at the minimum and maximum stresses typically differ by 20%–30%.

The compression curve for molybdenum was determined using the pressure determined by the gold marker at each angle. Equation of state data at 0° , 54.7° , and 90° are shown in Fig. 7 and Table II. The molybdenum equation of state at 54.7° is in reasonable agreement with hydrostatic compression curves constructed from extrapolation of ultrasonic elas-

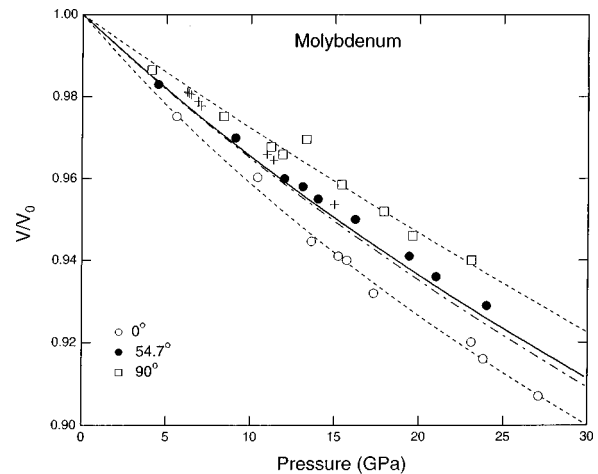


FIG. 7. Equation of state of molybdenum from lattice parameters measured at 0° , 54.7° , and 90° . The pressure is determined from the mean lattice parameter of gold. The dashed lines show Birch–Murnaghan equation fits to the data at 0° and 90° . The solid line shows the 300 K isotherm from ultrasonic data (Ref. 9), the dash-dot line shows the isotherm from high-pressure shock data (see Ref. 7), and the pluses are low-pressure shock data (see Ref. 12).

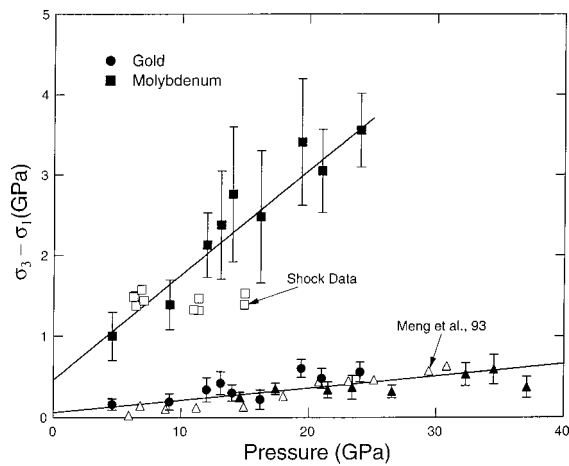


FIG. 8. Uniaxial stress component of gold (filled circles) and molybdenum (filled squares) as a function of pressure. Solid lines are least-squares fits to the data. For gold, open triangles are from Ref. 35 and filled triangles are from earlier radial diffraction data (see Ref. 26). For molybdenum, open symbols are yield strength measurements under shock compression (see Ref. 12).

ticity data⁹ and reduction of shock compression data using Mie–Grüneisen theory.⁷ Thus, it is possible to obtain a quasi-hydrostatic compression curve from these highly non-hydrostatic data by proper choice of the angle between the stress axis and the diffraction vector. However, the data at $\psi = 54.7^\circ$ show a slight systematic deviation from the isotherms with the diamond cell data being less compressible. A similar result was observed previously in a similar study using a rhenium–gold sample.²⁶ In that study, it was discussed that the deviation could be due to a variety of factors including the presence of local deviatoric stresses,^{31,34} error in static isotherms of sample or marker, pressure differences between the marker and sample, changes in sample positions as the angle is varied, or errors in setting $\psi = 0$.²³

Also shown in Fig. 7 are third-order Birch–Murnaghan equation fits to the data at 0° and 90° . The equations of state at the extreme angles yield equation of state parameters very different from expected values. The ambient-pressure isothermal bulk modulus K_0 of molybdenum is 261 GPa (Ref. 9) and its pressure derivative K'_0 is 4.0 (Ref. 7) to 4.5.⁹ The bulk moduli obtained from fits using the third-order Birch–Murnaghan equation at 0° and 90° are 210 and 348 GPa, respectively, a total variation of 65%. The pressure derivatives obtained from the inversions show even more extreme variation: from 1.8 at 90° to 5.8 at 0° . This illustrates the strong effect that nonhydrostaticity can have on equation of state parameters. This is also consistent with the behavior observed previously for rhenium.²⁶

The uniaxial stress component in gold was calculated using Eq. (15) and the pressure dependence of the shear modulus from Ref. 17 (Fig. 8). The results are in good agreement with earlier diamond cell data using the conventional axial x-ray geometry³⁵ as well as other radial diffraction data.²⁶ A linear fit to all the data from 5 to 37 GPa yields: $t = 0.06 + 0.015P$, where P is the pressure in GPa. The value of t obtained in this study ranges from 0.2 to 0.6 GPa at 5–24 GPa. The magnitude of the uniaxial stress component is less

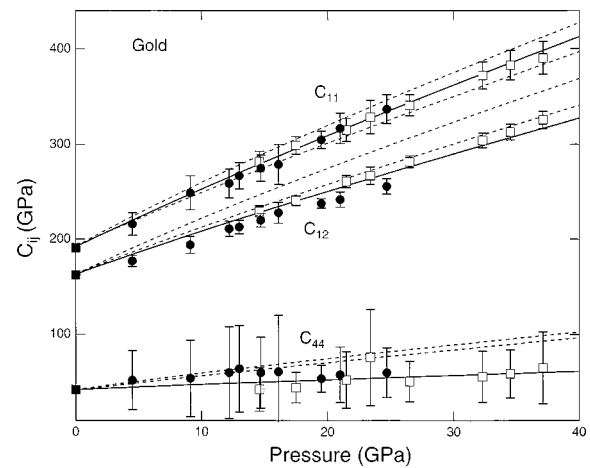


FIG. 9. Second-order elastic moduli of gold as a function of pressure. Filled circles are from this study. Open squares are from a rhenium/gold sample studied using the same technique (see Ref. 26). Error bars are one standard deviation. Solid lines are finite strain fits to the present data combined with that of Ref. 26 and ambient pressure data (see Ref. 17). The dashed lines show finite strain extrapolations of ultrasonic data (see Refs. 16 and 17), where the upper dashed curve corresponds to Ref. 16, and the lower dashed curve is from Ref. 17. The difference between adiabatic and isothermal moduli has been neglected.

than the uncertainty in the gold equation of state. The pressure error that results from using data at $\psi = 90^\circ$ is 0.5–1.7 GPa or about 10% over this pressure range. In general, the uniaxial stress values for gold in this experiment are slightly higher than found in an earlier experiment using the same geometry but for a sample mixed with rhenium.²⁶ The uniaxial stresses in molybdenum are also shown in Fig. 8. The shear modulus was obtained from ultrasonic data⁹ extrapolated to high pressure using finite strain theory.³³ For molybdenum, the uniaxial stress can be described by $t = 0.46 + 0.13P$.

The single-crystal elastic moduli calculated using Eqs. (12)–(14) are shown in Figs. 9 and 10. For gold, the results

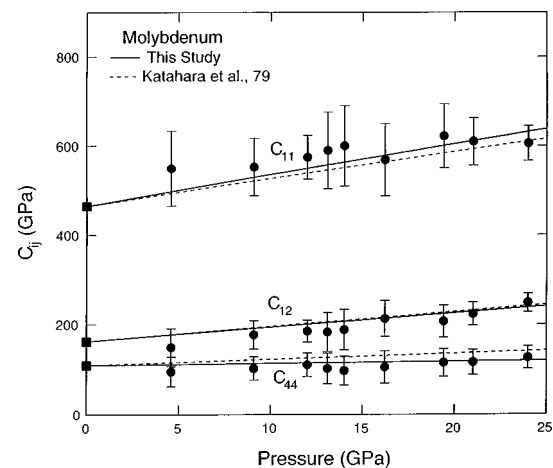


FIG. 10. Second-order elastic moduli of molybdenum as a function of pressure. The symbols are the present data and the solid lines are finite strain fits to the present data and ambient pressure data (filled squares) (see Ref. 9). The dashed lines show finite strain extrapolation of the pressure dependence of the moduli from ultrasonic data to 0.5 GPa (see Ref. 9). The difference between adiabatic and isothermal moduli has been neglected.

TABLE III. Pressure derivatives of second-order elastic moduli for gold and molybdenum.

Ref.	$\frac{\partial C_{11}}{\partial P}$	$\frac{\partial C_{12}}{\partial P}$	$\frac{\partial C_{44}}{\partial P}$
Gold			
This study ($\alpha=1$)	6.4	4.8	0.6
Ref. 16	7.0	6.1	1.8
Ref. 17	5.7	5.0	1.5
Ref. 18	6.7	5.9	1.8
Ref. 19	6.7	5.8	1.8
Molybdenum			
This study ($\alpha=1$)	7.3	3.3	0.5
Ref. 9	6.4	3.5	1.4

are compared with finite strain extrapolations³³ with two sets of ultrasonic elasticity data.^{16,17} Since the linear compressibilities and shear moduli used in Eqs. (12)–(14) were taken from the results of Ref. 17, a comparison with the lower dashed curve in Fig. 9 is most appropriate. Pressure derivatives obtained from finite strain fits to the x-ray elastic moduli combined with ambient pressure data are compared with ultrasonic pressure derivatives in Table III.

The results for gold are generally consistent with the x-ray elastic moduli in the previous gold–rhenium study,²⁶ although the values for C_{12} and C_{44} are slightly lower and higher, respectively, here than in the earlier study. The value of C_{44} shows very little pressure variation compared with extrapolation of ultrasonic elasticity values.

For molybdenum, the results are also in good agreement with the extrapolation of ultrasonic data.⁹ The shear modulus C_{44} again tends to lie slightly below ultrasonic values, although they are in agreement within uncertainties. Values of C_{11} and C_{12} tend to be slightly higher and lower, respectively, on decompression relative to measurements upon compression.

V. DISCUSSION

The elastic anisotropy of a cubic crystal can be characterized by the anisotropy ratio A , which is the ratio of shear moduli in the (100) and (110) planes in the [100] direction:

$$A = \frac{2C_{44}}{C_{11} - C_{12}} = \frac{2(S_{11} - S_{12})}{S_{44}} = 1 + \frac{2S}{S_{44}}. \tag{16}$$

An elastically isotropic material has $A=1$. Values of A greater than 1 signify that C_{44} is greater than $1/2(C_{11} - C_{12})$, whereas the opposite holds when A is less than 1.

For gold, the elastic anisotropy is large with $A=2.9$ at ambient pressure and extrapolation of ultrasonic data suggests this should increase weakly with pressure. In contrast, the elastic anisotropy of molybdenum is 0.72, implying that the shear velocity in the (110) plane is greater than the shear velocity in the (100) plane. The opposite orientations of the elastic anisotropy are responsible for different signs of the slopes observed in the $Q-3\Gamma$ plot (Fig. 6).

For the case where $\alpha=1$, Eqs. (12)–(14) yield

$$A = \frac{1}{1 + m_1/m_0}. \tag{17}$$

As discussed previously,^{23,26} the elastic anisotropy is strongly sensitive to the value of α . Using the values of m_0 and m_1 from Eqs. (12) and (13), we find that A for gold decreases from 2.9 at 4.6 GPa to 1.5 at 24.7 GPa. This decrease is largely due to the weak pressure dependence of C_{44} for $\alpha=1$. As discussed elsewhere,²⁶ the x-ray and ultrasonic data for gold at 14–37 GPa could be reconciled if α decreases from 1 near 14 GPa to about 0.5 at the highest pressure. The anisotropy of molybdenum from the x-ray moduli also decreases with pressure, but the magnitude of the effect is reduced. The anisotropy factor A varies from 0.5 at 4.6 GPa to 0.7 at 24.7 GPa. Extrapolation of high-pressure ultrasonic data for molybdenum suggests that A should be largely pressure independent for this material.

In this study, reducing α may also improve the agreement with ultrasonic data for gold at high pressure. For materials with $A > 1$, reducing α will decrease C_{11} and increase C_{12} and C_{44} with the strongest effect on C_{44} . As a result, the anisotropy factor A will increase. For materials with $A < 1$, decreasing α will also increase the anisotropy, causing A to decrease. For such materials, a reduction in α has the opposite effect on the individual moduli: C_{11} is increased and C_{12} and C_{44} are decreased. As a result, a reduction in α for molybdenum will result in poorer agreement between the x-ray elastic constants and ultrasonic data. Thus, reduction of α cannot simultaneously reconcile the low values of $\partial C_{44}/\partial P$ for x-ray data relative to ultrasonic data for both gold and molybdenum. The uncertainties in C_{44} are sufficiently large in this study that $\alpha=1$ is consistent with the current data set.

With further refinement, the present method offers a potential means to constrain α and, hence, better understand the nature of stress continuity across grain contacts in the high-pressure sample. This is an important issue as Reuss conditions are often assumed to hold when using an *in situ* pressure marker within the sample. There is evidence that low-pressure ultrasonic data may overpredict pressure derivatives of elastic moduli.²⁰ It is also now possible to directly measure elastic wave velocities to pressures above 10 GPa using ultrasonic techniques.³⁶ Such measurements are needed for gold and molybdenum to provide a more direct comparison with the results of this study.

The uniaxial stress values for molybdenum are compared to yield strength values determined under shock compression at 6.5–15 GPa in Fig. 8. The shock data¹² were obtained by comparing the Hugoniot $P-V$ states to the inferred hydrostat from ultrasonic data.⁹ The uniaxial stress values under static compression are in agreement with the shock yield strengths at these pressures (Fig. 8). The dynamic yield strengths, however, appear to exhibit little or no pressure dependence in contrast to the static uniaxial stress. In general, dynamic yield strengths increase with compression until very high pressures where shock heating effects become important.¹⁰ The temperature dependence of the yield strength at the Hugoniot elastic limit for shocked molybdenum was determined to be -0.0004 GPa/K from com-

parison of room-temperature measurements with those from a 1400 °C initial state.¹³ The yield strength of a material depends on strain rate and total strain. For molybdenum, the 1 bar yield strength at a strain rate of $<1 \text{ s}^{-1}$, which is appropriate for diamond cell experiments, is 0.7 GPa.³⁷ This value is consistent with the trend obtained from our data.

A comparison of shock and static yield strengths has implications for the ruby pressure scale. At pressures of 10–20 GPa, the shock and static strengths are roughly similar, and strength effects are likely to cancel out in the reduction of shock data to a static isotherm. This can be seen with reference to Fig. 7, which shows that molybdenum shock P – V states are similar to diamond cell values taken under nonhydrostatic compression at 90° in this compression range. At higher pressures, the situation is less clear as the pressure dependence of the shock strength is not well constrained. Molybdenum was used to calibrate the ruby scale up to 95.4 GPa (Ref. 1) and shock temperatures are expected to range from 300 to 1100 K over this interval.⁷ Thermal softening under shock compression is, therefore, likely to be modest, and near cancellation of static and dynamic strength effects may hold over this entire range. Using molybdenum as an *in situ* standard at ultrahigh pressures may be problematic, however. In this case, the dynamic yield strength may be small due to intense shock heating, while the static yield strength could be very large if the trend shown in Fig. 8 continues to high pressure.

VI. SUMMARY

Nonhydrostatic stress can strongly affect the measured lattice strains in a diamond-anvil cell. By using a beryllium gasket and x-ray diffraction to measure lattice strains as a function of angle ψ from the diamond cell axis, valuable additional information can be obtained on the state of the high-pressure sample. Here, we have examined gold and molybdenum at 5–24 GPa. The results for gold are consistent with an earlier study using the same technique. The uniaxial stress supported within gold is 0.2–0.6 GPa at these pressures. When gold is used as a pressure marker with a conventional axial x-ray geometry, the pressure is underestimated by $\sim 10\%$. The single-crystal elastic moduli for gold are generally consistent with ultrasonic values, although the pressure dependence of C_{44} is less than obtained from low-pressure ultrasonic data. For molybdenum, the uniaxial stress is given by $t = 0.46 + 0.13P$, where P is the pressure in GPa. It is found that the equation of state of molybdenum is strongly dependent on ψ with bulk modulus values that vary by 66% as ψ increases from 0° to 90°. The elastic moduli of molybdenum are in good agreement with extrapolated ultrasonic values. However, the pressure dependence of C_{44} for molybdenum is also less than that obtained from low-pressure ultrasonic data.

ACKNOWLEDGMENTS

The authors thank Kevin Long and Kunal Bose for assistance in data processing, and Yanbin Wang for experimental assistance. This research was supported by the Na-

tional Science Foundation. Portions of this work were performed at GeoSoilEnviroCARS (GSECARS), Sector 13, Advanced Photon Source at Argonne National Laboratory. GSECARS is supported by the National Science Foundation — Earth Sciences, Department of Energy — Geosciences, W. M. Keck Foundation, and the United States Department of Agriculture. Use of the Advanced Photon Source was supported by the U.S. Department of Energy, Basic Energy Sciences, Office of Energy Research, under Contract No. W-31-109-Eng-38.

- ¹H. K. Mao, P. M. Bell, J. W. Shaner, and D. J. Steinberg, *J. Appl. Phys.* **49**, 3276 (1978).
- ²R. S. Hixson, D. A. Boness, J. W. Shaner, and J. A. Moriarty, *Phys. Rev. Lett.* **62**, 637 (1989).
- ³Y. K. Vohra and A. L. Ruoff, *Phys. Rev. B* **42**, 8651 (1990).
- ⁴B. K. Godwal and R. Jeanloz, *Phys. Rev. B* **41**, 7440 (1990).
- ⁵J. A. Moriarty, *High Press. Res.* **13**, 343 (1995).
- ⁶N. E. Christensen, A. L. Ruoff, and C. O. Rodriguez, *Phys. Rev. B* **52**, 9121 (1995).
- ⁷R. G. McQueen, S. P. Marsh, J. W. Taylor, J. N. Fritz, and W. J. Carter, in *High-Velocity Impact Phenomena*, edited by R. Kinslow (Academic, San Diego, CA, 1970), p. 294.
- ⁸R. S. Hixson and J. N. Fritz, *J. Appl. Phys.* **71**, 1721 (1992).
- ⁹K. W. Katahara, M. H. Manghnani, and E. S. Fisher, *J. Phys. F* **9**, 773 (1979).
- ¹⁰J. R. Asay and G. I. Kerley, *Int. J. Impact Eng.* **5**, 69 (1987).
- ¹¹G. I. Kanel, *J. Mech. Phys. Solids* **46**, 1869 (1998).
- ¹²M. D. Furnish and L. C. Chhabildas, in *High Strain Rate Behavior of Refractory Metals and Alloys*, edited by R. Asfahani, E. Chen, and A. Crowson (The Minerals, Metals, and Materials Society, Warrendale, PA, 1992), p. 229.
- ¹³T. S. Duffy and T. J. Ahrens, *J. Appl. Phys.* **76**, 835 (1994).
- ¹⁴D. L. Heinz and R. Jeanloz, *J. Appl. Phys.* **55**, 885 (1984).
- ¹⁵P. M. Bell, J. Xu, and H. K. Mao, in *Shock Waves in Condensed Matter*, edited by Y. Gupta (Plenum, New York, 1986), p. 125.
- ¹⁶W. B. Daniels and C. S. Smith, *Phys. Rev.* **111**, 713 (1958).
- ¹⁷Y. Hiki and A. Granato, *Phys. Rev.* **144**, 411 (1966).
- ¹⁸B. Golding, S. C. Moss, and B. L. Averbach, *Phys. Rev.* **158**, 637 (1967).
- ¹⁹S. N. Biswas, P. Van't Klooster, and N. J. Trappeniers, *Physica B & C* **103**, 235 (1981).
- ²⁰T. S. Duffy and Y. Wang, *Rev. Mineral.* **37**, 425 (1998).
- ²¹A. K. Singh, *J. Appl. Phys.* **73**, 4278 (1993).
- ²²A. K. Singh, *J. Appl. Phys.* **74**, 5920 (1993).
- ²³A. K. Singh, C. Balasingh, H. K. Mao, R. J. Hemley, and J. Shu, *J. Appl. Phys.* **83**, 7567 (1998).
- ²⁴A. K. Singh, H. K. Mao, J. Shu, and R. J. Hemley, *Phys. Rev. Lett.* **80**, 2157 (1998).
- ²⁵H. K. Mao, J. Shu, G. Shen, R. J. Hemley, B. Li, and A. K. Singh, *Nature (London)* **396**, 741 (1998).
- ²⁶T. S. Duffy, G. Shen, D. L. Heinz, J. Shu, Y. Ma, H. K. Mao, and R. J. Hemley, *Phys. Rev. B* (in press).
- ²⁷T. Uchida, N. Funamori, and T. Yagi, *J. Appl. Phys.* **80**, 739 (1996).
- ²⁸J. F. Nye, *Physical Properties of Crystals* (Oxford University Press, London, 1975).
- ²⁹H. K. Mao and R. J. Hemley, *Rev. Mineral.* **37**, 1 (1998).
- ³⁰M. L. Rivers, T. S. Duffy, Y. Wang, P. J. Eng, S. R. Sutton, and G. Shen, in *Properties of Earth and Planetary Materials at High Pressure and Temperature*, edited by M. H. Manghnani and T. Yagi (American Geophysical Union, Washington, DC, 1998), p. 79.
- ³¹N. Funamori, M. Funamori, R. Jeanloz, and N. Hamaya, *J. Appl. Phys.* **82**, 142 (1997).
- ³²D. J. Weidner, *Rev. Mineral.* **37**, 493 (1998).
- ³³F. Birch, *J. Geophys. Res.* **83**, 1257 (1978).
- ³⁴D. J. Weidner, Y. Wang, and M. T. Vaughan, *Geophys. Res. Lett.* **21**, 753 (1994).
- ³⁵Y. Meng, D. J. Weidner, and Y. Fei, *Geophys. Res. Lett.* **20**, 1147 (1993).
- ³⁶R. C. Liebermann and B. Li, *Rev. Mineral.* **37**, 459 (1998).
- ³⁷D. J. Steinberg, *J. Appl. Phys.* **74**, 3827 (1993).